

Inchworm Monte Carlo for exact non-adiabatic dynamics I. Theory and algorithms

Hsing-Ta Chen,^{1,2} Guy Cohen,^{2,3} and David R. Reichman¹

¹*Department of Chemistry, Columbia University, New York, New York 10027, U.S.A.*

²*The Raymond and Beverly Sackler Center for Computational Molecular and Materials Science, Tel Aviv University, Tel Aviv 69978, Israel*

³*School of Chemistry, The Sackler Faculty of Exact Sciences, Tel Aviv University, Tel Aviv 69978, Israel*

In this paper we provide a detailed description of the inchworm Monte Carlo formalism for the exact study of real-time non-adiabatic dynamics. This method optimally recycles Monte Carlo information from earlier times to greatly suppress the dynamical sign problem. Using the example of the spin–boson model, we formulate the inchworm expansion in two distinct ways: The first with respect to an expansion in the system–bath coupling and the second as an expansion in the diabatic coupling. The latter approach motivates the development of a cumulant version of the inchworm Monte Carlo method, which has the benefit of improved scaling. This paper deals completely with methodology, while the companion paper provides a comprehensive comparison of the performance of the inchworm Monte Carlo algorithms to other exact methodologies as well as a discussion of the relative advantages and disadvantages of each.

I. INTRODUCTION

The description of real-time dynamics in many-body quantum systems continues to provide major challenges for current research. An accurate theoretical understanding of nonequilibrium processes ranging from charge and energy transport in quantum dots and molecular junctions¹ to laser-induced electronic phase transformations² is crucial for the interpretation of experimental results and the eventual design of new materials and technologies. Quantum Monte Carlo (QMC) techniques form the basis for the exact description of the *thermodynamics* of systems dominated by quantum fluctuations.³ In this setting, a variety of QMC methods may be used to *exactly* calculate the properties of lattice and continuum systems, including systems where boson particle statistics induce non-trivial collective phenomena such as the transition to a superfluid state.^{4–6} The inclusion of fermionic statistics within QMC is more difficult, reflecting the NP-hardness of the generic electronic structure problem.⁷ This difficulty reveals itself in the “fermionic sign problem,” where Monte Carlo summands alternate sign, leading to a poor signal-to-noise ratio that can inhibit the accurate calculation of the thermodynamic properties of fermionic assemblies. Despite this difficulty, the umbrella of QMC techniques has essentially solved the problem of the thermodynamics of non-fermionic systems,^{8–11} while great progress continues to be made towards the development of accurate QMC approaches for fermions.^{12–19}

The simulation of real-time quantum dynamics presents another layer of difficulty that is absent when thermodynamics alone is considered. In general, when considering the exact simulation of quantum dynamics, the computational cost scales exponentially with increasing time. This poor scaling manifests in distinct ways in different methodologies.^{20–27} Within attempts to extend

QMC to the real-time axis, exponentially poor scaling arises from the oscillating phase factors generated by the time evolution operator e^{-iHt} . The summation of random phase information leads to a shrinking signal to noise ratio known as the “dynamical sign problem”. This afflicts all dynamical QMC simulations, regardless of the nature of the underlying particle statistics.^{16–19}

Modern diagrammatic variants of QMC (dQMC) have proven extremely powerful in the study of thermodynamic properties of impurity models, which consist of a small interacting subsystem coupled to noninteracting fermionic or bosonic baths.²⁷ The extension of these approaches to real-time dynamics has also met with some success.^{21–24,28,29} In particular, in conjunction with partial resummations of the exact diagrammatic series^{26,27} and reduced dynamics techniques,^{30,31} real-time dQMC has proven capable of the exact simulation of nonequilibrium properties in the paradigmatic Anderson model for non-trivial time scales in select parameter regimes.³² Despite the aforementioned successes, previous real-time dQMC methods have all been plagued by the dynamical sign problem to differing degrees.^{26,33–37} Very recently, a new dQMC method, dubbed the “inchworm algorithm,” has been introduced that largely overcomes the dynamical sign problem.³⁸ The inchworm algorithm optimally recycles diagrammatic information so that the computational cost scales approximately quadratically, as opposed to exponentially, with time. For the case of the Anderson model, the inchworm algorithm has enabled exact real-time simulation even deep within strongly correlated regions of the parameter space, such as the Kondo and mixed valence regimes.

While progress for the Anderson model has been impressive, it should be noted that the number and range of exact benchmarks for this model are far fewer than those available for a simpler impurity model: the spin–boson model. The spin–boson model consists of a two-level system coupled linearly to a bosonic bath, and constitutes

the basic proxy for dissipative condensed phase charge and energy transfer problems.^{39–41} Two decades of numerical effort aimed at the spin–boson problem have produced a suite of methodologies capable of long-time simulation of nonequilibrium observables over essentially the entire parameter space of the model.^{16,33,34,42–49} In this sense, the spin–boson model embodies a stringent test which should be passed by any new numerically exact approach to real-time quantum dynamics.

In the following work, we use the spin–boson model as a platform to provide the essential details of the inchworm approach and to improve and expand upon the methodology. In particular we describe two diagrammatic expansions (and their resummations within the inchworm framework) rooted in distinct exactly solvable reference systems. We further introduce a new cumulant-based approach^{50–53} that reduces the computational cost from quadratic to linear in time. In essence, the use of cumulants allows for the construction of an inchworm expansion for the memory function directly from the moment expansion and without the need for any *a priori* information about the memory kernel itself. We argue that taken together, the distinct inchworm algorithms presented here should essentially cover the relevant parameter space of the spin–boson model. We defer the detailed comparison of our new approach to established benchmarks, as well as a discussion of the relative benefits and drawbacks of our approach, to a companion paper.

The organization of the paper is as follows. In Sec. II, we review the real-time dQMC scheme and the inchworm algorithm in a general formalism. In Sec. III, we formulate the system–bath coupling expansion and its corresponding inchworm expansion. In Sec. IV, the diabatic coupling expansion is described. In Sec. V, we introduce cumulant inchworm expansions based on the diabatic coupling expansion. Our conclusions are presented in Sec. VI.

II. DQMC SCHEME AND THE INCHWORM ALGORITHM

In this section, we briefly review the real-time dQMC approach,²⁷ the emergence of the dynamical sign problem and the inchworm algorithm³⁸ in a general framework.

We consider a generic Hamiltonian of an open quantum system in the form

$$H = H_s + H_b + H_{sb}, \quad (1)$$

where H_s and H_b are the Hamiltonian of the system and the bath, respectively, and H_{sb} describes the system–bath coupling. For a given observable O , we are interested in its time-dependent expectation value

$$\langle O(t) \rangle = \text{Tr} \{ \rho_0 e^{iHt} O e^{-iHt} \}. \quad (2)$$

Here, $\langle \cdot \rangle = \text{Tr} \{ \rho_0 \cdot \}$ is the trace performed over all degrees of freedom and ρ_0 is the initial density matrix of

the full system. It should be noted that equilibrium time correlation functions may also be calculated within the framework outlined below,^{32,36} however for simplicity we focus on one-time non-equilibrium quantities of the form (2).

A. Dyson series

To evaluate the dynamics of the observable $\langle O(t) \rangle$, a key needed element is the propagator e^{-iHt} , which is difficult to calculate in a computationally useful form. In general, we can expand the propagator in a perturbative fashion by writing the Hamiltonian as

$$H = H_0 + H', \quad (3)$$

thus partitioning H into a (solvable) H_0 and an interaction Hamiltonian H' . In this interaction picture, the dynamics of an operator O is given by

$$e^{iHt} O e^{-iHt} = U^\dagger(t) \tilde{O}(t) U(t), \quad (4)$$

where the propagator is $U(t)$ given by $U(t) = e^{iH_0 t} e^{-iHt}$. We denote the time-dependent operator in the interaction picture by $\tilde{O}(t) = e^{iH_0 t} O e^{-iH_0 t}$. One can expand the propagator using the time-ordered Dyson series ($\hbar = 1$)

$$U(t) = \sum_{n=0}^{\infty} (-i)^n \int_0^t dt_1 \int_0^{t_1} dt_2 \cdots \int_0^{t_{n-1}} dt_n \times \tilde{H}'(t_1) \tilde{H}'(t_2) \cdots \tilde{H}'(t_n) \quad (5)$$

which contains a series of interaction operators $\tilde{H}'(t_i) = e^{iH_0 t} H' e^{-iH_0 t}$ with the chronological time ordering $t > t_1 > t_2 > \cdots > t_n > 0$. If this expansion is applied to the two interaction picture propagators in Eq. 4, the folded Keldysh contour naturally emerges from the sequence of interaction operators generated by the product. The interaction operators arising from $U(t)$ have time arguments denoted as $\{t_i^+\}$, and are thought of as existing on the forward or $+$ branch of the contour, while those emanating from $U^\dagger(t)$ have time arguments denoted as $\{t_i^-\}$, and exist on the backward or $-$ branch. This is illustrated in Fig. 1a. The contour is folded at $t = t_{\max}$, where the observable operator is applied. Each set of time arguments, $\{t_i^+\}$ and $\{t_i^-\}$, is time ordered: $t_{\max} > t_1^\pm > t_2^\pm > \cdots > 0^\pm$, where 0^\pm denote the initial time on the \pm branch, respectively. Therefore, we can write Eq. 4 as

$$O(t) = \sum_{n=0}^{\infty} \int_0^{t_{\max}} dt_1^+ \int_0^{t_1^+} dt_2^+ \cdots \int_0^{t_{n-1}^+} dt_n^+ \times \sum_{n'=0}^{\infty} \int_0^{t_{\max}} dt_1^- \int_0^{t_1^-} dt_2^- \cdots \int_0^{t_{n'-1}^-} dt_{n'}^- \times \quad (6)$$

$$(-i)^n i^{n'} \tilde{H}'(t_n^+) \cdots \tilde{H}'(t_1^+) \times \tilde{O}(t_{\max}) \tilde{H}'(t_1^-) \cdots \tilde{H}'(t_{n'}^-).$$

For brevity, it will be convenient to write the two types of time arguments on the two branches of the contour in terms of a single time argument label s_i :

$$s_i = \begin{cases} s_i^+ = t_{n-i+1}^+ & i \leq n, \\ s_i^- = t_{i-n}^- & n < i \leq m. \end{cases} \quad (7)$$

Here, $m = n + n'$ and $\{s_i\}$ is ordered according to the Keldysh contour causality, $s_1 < \dots < s_m$ as shown in Fig. 1. We define $s_i < s_j$ if s_i occurs before s_j on the Keldysh contour. Therefore, we can write Eq. 4 as an expansion in terms of s_i ,

$$O(t) = \sum_{m=0}^{\infty} \sum_{n=0}^m \int ds_m \dots \int ds_1 (-1)^n i^m \times \tilde{H}'(s_m) \dots \tilde{H}'(s_{n+1}) \tilde{O}(t_{\max}) \tilde{H}'(s_n) \dots \tilde{H}'(s_1), \quad (8)$$

where the integration $\int ds_m \dots \int ds_1$ is taken to represent

$$\int ds_m \dots \int ds_1 = \int_0^{t_{\max}} dt_1^+ \int_0^{t_1^+} dt_2^+ \dots \int_0^{t_{n-1}^+} dt_n^+ \int_0^{t_{\max}} dt_1^- \int_0^{t_1^-} dt_2^- \dots \int_0^{t_{n'-1}^-} dt_{n'}^-. \quad (9)$$

Each term in the expansion can be represented by diagrams, in which a vertex or open circle in Fig. 1(a) represents the interactions occurring at the times $\{s_i\}$ and a cross symbol indicates the tip or the folding time t_{\max} of the Keldysh contour where the observable operator acts. For instance, Fig. 1b shows the diagrams of the unperturbed term ($m = 0$) and some example diagrams of second order ($m = 2$, two vertices) and of fourth order ($m = 4$, four vertices).

B. Real-time path integral formulation

The dynamical quantities of interest can be expressed in the form of a path integral, or more generally the integral over the contour configuration space

$$\langle O(t) \rangle = \int d\mathbf{s} \mathcal{O}(\mathbf{s}), \quad (10)$$

where we denote $\mathbf{s} = \{s_i\}$ as the contour configuration. Note that this expression is implicitly time-ordered and the integration $\int d\mathbf{s}$ is taken to mean

$$\int d\mathbf{s} = \sum_{m=0}^{\infty} \sum_{n=0}^m \int ds_m \dots \int ds_1. \quad (11)$$

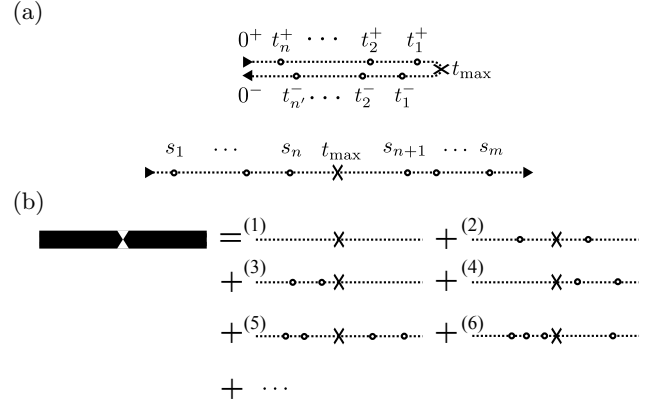


Figure 1. (a) A configuration \mathbf{s} drawn on the Keldysh contour, with physical times t_i on the forward or $+$ branch and t'_i on the backward or $-$ branch. Below, the configuration is shown on the unfolded contour with contour times s_i . The \times indicates the tip or fold of the contour and the ticks indicate interaction operators H' . (b) General framework of bare dQMC. The thin line represents an unperturbed propagator $e^{-iH_0 s}$, while the thick line represents the exact sum over all possible configurations contributing to some observable $\langle O(t) \rangle$. (1) is the zeroth ($m = 0$) order contribution, $\langle e^{iH_0 t} O e^{-iH_0 t} \rangle$. (2)–(4) are examples of second ($m = 2$) order contributions with (2) $n = 1$, (3) $n = 2$, and (4) $n = 0$. (5) and (6) are examples of fourth ($m = 4$) order configurations.

The contribution of a given configuration \mathbf{s} is given by

$$\mathcal{O}(\mathbf{s}) = (-1)^n i^m \left\langle \tilde{H}'(s_m) \dots \tilde{H}'(s_{n+1}) \times \tilde{O}(t_{\max}) \tilde{H}'(s_n) \dots \tilde{H}'(s_1) \right\rangle. \quad (12)$$

This object is a seemingly complicated multi-time quantity, but in many cases is that it can be efficiently evaluated since it is defined by an interaction picture under the propagation associated with a solvable H_0 .

The dQMC method provides an unbiased estimator for the infinite-dimensional integral over all configuration parameters, $\int d\mathbf{s} \mathcal{O}(\mathbf{s})$, by summing over a set of sample configurations \mathbf{s}_i drawn from some normalized probability distribution defined by $\text{Prob}(\mathbf{s}) = \frac{w(\mathbf{s})}{\int d\mathbf{s} w(\mathbf{s})} \equiv \frac{w(\mathbf{s})}{Z_w}$. The Metropolis–Hastings algorithm^{54,55} is method for generating a sample set of this type when only $w(\mathbf{s})$ is known. To see how this is used, consider that for any prescribed weight function $w(\mathbf{s})$, we have

$$\int d\mathbf{s} \mathcal{O}(\mathbf{s}) = Z_w \int d\mathbf{s} \frac{\mathcal{O}(\mathbf{s})}{w(\mathbf{s})} \text{Prob}(\mathbf{s}). \quad (13)$$

Given that the $\{s_i\}$ for $i \in \{1, \dots, M\}$ are drawn from $\text{Prob}(\mathbf{s})$, in the limit of large M one obtains

$$\int d\mathbf{s} \mathcal{O}(\mathbf{s}) \simeq \frac{Z_w}{M} \sum_{i=1}^M \frac{\mathcal{O}(\mathbf{s}_i)}{w(\mathbf{s}_i)} \equiv Z_w \left\langle \frac{\mathcal{O}}{w} \right\rangle_w. \quad (14)$$

Importantly, we note that Z_w is completely independent of the observable calculated. Therefore, to remove the

dependence on Z_w , we introduce a “normalizing” observable $N = \int d\mathbf{s} \mathcal{N}(\mathbf{s})$ which can be evaluated analytically. Evaluating N via the same Monte Carlo procedure, one obtains

$$N = \int d\mathbf{s} \mathcal{N}(\mathbf{s}) \simeq Z_w \left\langle \frac{\mathcal{N}}{w} \right\rangle_w. \quad (15)$$

With this normalization, Z_w cancels out of all final expressions:

$$\int d\mathbf{s} \mathcal{O}(\mathbf{s}) = N \frac{\int d\mathbf{s} \mathcal{O}(\mathbf{s})}{\int d\mathbf{s} \mathcal{N}(\mathbf{s})} \simeq N \frac{Z_w \left\langle \frac{\mathcal{O}}{w} \right\rangle_w}{Z_w \left\langle \frac{\mathcal{N}}{w} \right\rangle_w} = N \frac{\left\langle \frac{\mathcal{O}}{w} \right\rangle_w}{\left\langle \frac{\mathcal{N}}{w} \right\rangle_w}. \quad (16)$$

Since we have complete freedom in the choice of N , one is free to choose a quantity which is easy to evaluate in both the Monte Carlo and the analytical calculation. The choice used here is $\mathcal{N}(\mathbf{s}) = 1$, such that N is simply the hypervolume of the multidimensional space of interaction times. Since this hypervolume normalization is positive definite, it cannot have a sign problem, and all potential sign problems must appear in the nominator. For $w(\mathbf{s})$, we typically choose the absolute value $|\mathcal{O}(\mathbf{s})|$ of the contribution to the observable itself or a closely related property, such that the summation is optimized for summing large contributions to a particular observable. It is currently unknown whether this choice is optimal.

C. Dynamical sign problem and inchworm algorithms

Unfortunately, summing individual contributions to an observable in this manner, the so-called *bare* dQMC algorithm, generally involves a dynamical sign problem. In real-time dQMC, the dynamical sign problem is caused by the oscillatory nature of real-time propagators which results in exponentially growing computational cost as time increases.^{21,22,28,56} To circumvent the dynamical sign problem, we employ inchworm expansions.³⁸ This allows us to efficiently reuse quantities propagated within short time intervals in the calculation of quantities propagated between longer times. Two concrete examples of practical inchworm algorithms for the spin-boson model will be developed below.

We briefly introduce the general concept behind inchworm expansions. Let $s_i < s_\uparrow < s_f$ be three times: an “initial,” “inchworm” and “final” time, respectively. Assume some set of properties have been exactly evaluated for all cases where all interaction vertices are restricted to the time interval $[s_i, s_\uparrow]$. Given knowledge of these auxiliary restricted quantities, it is often possible to construct an efficient expansion for the same set of quantities with the vertices restricted to the *longer* interval $[s_i, s_f]$. This describes an *inchworm step*, or the process of *inching*. A series of inchworm steps allows one to start with a set of easily evaluated restricted quantities defined over very short intervals, eventually obtaining the set of unrestricted physical quantities for which interaction vertices span the full length of the Keldysh contour.

The inchworm algorithm has the distinct advantage (when compared to its bare equivalent) that much fewer diagrams must be sampled to obtain a converged answer, since each inchworm diagram contains an infinite number of bare diagrams. Often, relatively few low-order inchworm diagrams contain all important contributions from the relevant bare diagrams at all orders. This advantage comes at two important costs. First, as when working with nonequilibrium Green’s functions, one is forced to calculate a complete set of two-time properties even if only single-time properties are of interest. Specifically, all propagators between any two points in $[s_i, s_f]$ are required to obtain a propagator between s_i and s_f . Second, Monte Carlo evaluations at long times are no longer independent of short-time evaluations, and errors are carried forward in time during the stepping procedure. This has profound computational implications in that the algorithm is not “embarrassingly parallel” like standard Monte Carlo techniques, since information concerning short-time propagators must be distributed between the various computer nodes performing the calculation. Furthermore, careful error analysis is required in order to take error propagation into account. Essentially, a series of completely independent calculations must be carried out to evaluate the statistical errors, and one must then verify that systematic errors due to the error propagation (in addition to the statistical ones common to all Monte Carlo techniques) are assessed and converged to within the desired accuracy.

Within the formulation of inchworm algorithm, each single inchworm step is numerically exact, in the sense that unbiased results are obtained with only statistical errors that can be converged to any desired accuracy by increasing the number of Monte Carlo samples. The sequence/grid of inchworm steps with finite size becomes exact at the limit of small time discretization, where all propagators between shorter time intervals can be interpolated into a smooth functional form which accurately represents the exact continuous propagator. In practice, it is usually also necessary to truncate (and converge in) the maximum order of sampled configuration for each inchworm step. A more detailed discussion and a sequence of tests will be presented in the companion paper.

D. Spin-boson model

We now specialize the discussion to the case of the spin-boson model. This allows us to give explicit expressions for the terms that emerge in expansions that employ different choices of H_0 . The form of the Hamiltonian is given by Eq. (1). The system Hamiltonian H_s is taken to be a two-level system in the diabatic basis $|\alpha\rangle \in \{|1\rangle, |2\rangle\}$,

$$H_s = \epsilon \hat{\sigma}_z + \Delta \hat{\sigma}_x. \quad (17)$$

In this notation, $\hat{\sigma}_z = |1\rangle\langle 1| - |2\rangle\langle 2|$ and $\hat{\sigma}_x = |1\rangle\langle 2| + |2\rangle\langle 1|$. The energetic bias ϵ is the energy difference be-

tween the two diabatic states, and the diabatic coupling Δ characterizes spin flip processes within the electronic system. The boson bath consists of a set of harmonic oscillators with frequencies ω_ℓ described by the bath Hamiltonian

$$H_b = \sum_\ell \frac{1}{2} (p_\ell^2 + \omega_\ell^2 x_\ell^2) = \sum_\ell \omega_\ell \left(b_\ell^\dagger b_\ell + \frac{1}{2} \right). \quad (18)$$

The system–bath coupling H_{sb} is assumed to be linear in the bath coordinates

$$H_{sb} = \hat{\sigma}_z \sum_\ell c_\ell x_\ell. \quad (19)$$

The coupling constants c_ℓ describe the strength of the interaction between the harmonic modes and the spin. The system–bath coupling is typically parametrized in compact form by the spectral density

$$J(\omega) = \frac{\pi}{2} \sum_\ell \frac{c_\ell^2}{\omega_\ell} \delta(\omega - \omega_\ell). \quad (20)$$

Throughout this work, we will concentrate on the local dynamics of the spin $\hat{\sigma}_z$ in the diabatic basis

$$\langle \sigma_z(t) \rangle = \text{Tr} \{ \rho_0 e^{iHt} \hat{\sigma}_z e^{-iHt} \}. \quad (21)$$

Here we only address factorized initial conditions corresponding to thermal equilibrium of the bath in the absence of the system–bath coupling, such that the initial density matrix is given by the factorized form $\rho_0 = \rho_s \otimes \rho_b$, with the bath initially in equilibrium $\rho_b = \frac{e^{-\beta H_b}}{\text{Tr}_b \{ e^{-\beta H_b} \}}$. We specify the initial condition of the spin as $\rho_s = |1\rangle \langle 1|$. Treatment of more general initial conditions is simple but will not be discussed further here.

There are several useful ways of partitioning H into H_0 and H' such that the perturbation series of Eq. 3 can be carried out, each yielding a different type of expansion. We will discuss two such choices. One treatment takes $H' = H_{sb}$, expanding with respect to the system–bath coupling. Another takes $H' = \Delta \hat{\sigma}_x$, expanding in the diabatic coupling Δ . In the following sections, we discuss these expansions and their inchworm Monte Carlo implementations.

III. SYSTEM–BATH COUPLING INCHWORM (SBCI) EXPANSION

A. Bare dQMC

We start with the example of the bare dQMC expansion in terms of the system–bath coupling $H' = H_{sb}$. This expansion is analogous to the hybridization expansion in the Anderson model, for which the first inchworm expansion was formulated. The unperturbed Hamiltonian is taken to be $H_0 = H_s + H_b$ and the initial density

matrix is $\rho_0 = |1\rangle \langle 1| \otimes \rho_b$. To write a dQMC expression for the expectation value of the observable $O = \hat{\sigma}_z$, we must determine the contribution $\mathcal{O}(\mathbf{s})$ of any given configuration \mathbf{s} to this expectation value in the form of Eq. 12:

$$\mathcal{O}(\mathbf{s}) = (-1)^n i^m \left\langle \tilde{H}_{sb}(s_m) \cdots \tilde{H}_{sb}(s_{n+1}) \times \tilde{\sigma}_z(t) \tilde{H}_{sb}(s_n) \cdots \tilde{H}_{sb}(s_1) \right\rangle. \quad (22)$$

In the interaction picture $\tilde{H}_{sb}(s) = e^{iH_0 s} H_{sb} e^{-iH_0 s}$ can be factorized as

$$\tilde{H}_{sb}(s) = \tilde{\sigma}_z(s) \times \sum_\ell c_\ell \tilde{x}_\ell(s), \quad (23)$$

and we define the operator of the bath part as

$$\tilde{B}(s) = \sum_k c_k \tilde{x}_k(s). \quad (24)$$

It turns out that for a linear coupling of the form of Eq. (19), one can write Eq. (22) as a product of a system influence functional $\mathcal{U}(\mathbf{s})$ and a bath influence functional $\mathcal{L}(\mathbf{s})$:

$$\mathcal{O}(\mathbf{s}) = (-1)^n i^m \mathcal{U}(\mathbf{s}) \mathcal{L}(\mathbf{s}). \quad (25)$$

The system influence functional $\mathcal{U}(\mathbf{s})$ for the given initial condition $|1\rangle \langle 1|$ is defined as

$$\mathcal{U}(\mathbf{s}) = \langle 1 | \tilde{\sigma}_z(s_m) \cdots \tilde{\sigma}_z(s_{n+1}) \times \tilde{\sigma}_z(t_{\max}) \tilde{\sigma}_z(s_n) \cdots \tilde{\sigma}_z(s_1) | 1 \rangle. \quad (26)$$

For the spin- $\frac{1}{2}$ case, all operators can be written in the form of matrices of rank 2 in the basis of the Hilbert space of the isolated spin. Eq. (26) can then be efficiently evaluated as a matrix product of unperturbed system propagators of the form $e^{-iH_s(s_i - s_{i-1})}$, sandwiched between $\hat{\sigma}_z$ operators with $s_i - s_j$ denoting the difference of physical times given by Eq. (7).

The bath influence functional is given by an m -time interaction picture correlation function of the bath operator $\tilde{B}(s)$ in the form of

$$\mathcal{L}(\mathbf{s}) = \left\langle \tilde{B}(s_m) \cdots \tilde{B}(s_1) \right\rangle_b, \quad (27)$$

where we denote $\langle \cdot \rangle_b = \text{Tr}_b \{ \rho_b \cdot \}$ and ρ_b is the initial bath density matrix. Using Wick's theorem, which is valid for the bath operators within the interaction picture, one can express $\mathcal{L}(\mathbf{s})$ as a sum of products of two-time correlation functions by use of the identity

$$\left\langle \tilde{B}(s_m) \cdots \tilde{B}(s_1) \right\rangle_b = \sum_{q \in \mathcal{Q}_m} \prod_{(j,k) \in q} \left\langle \tilde{B}(s_k) \tilde{B}(s_j) \right\rangle_b. \quad (28)$$

The bath influence functional is zero for odd m . \mathcal{Q}_m denotes the set of possible distinct pairings of the integers 1, 2, ..., m : each element $q \in \mathcal{Q}_m$ is a set of ordered tuples

corresponding to a single pairing. For example, for $m = 2$ there is only one pairing, $q = \{(2, 1)\}$, and

$$\mathcal{Q}_2 = \{\{(1, 2)\}\}.$$

For $m = 4$ there are three possible pairings:

$$\mathcal{Q}_4 = \{\{(1, 2), (3, 4)\}, \{(1, 3), (2, 4)\}, \{(1, 4), (2, 3)\}\},$$

and so on. With these definitions, the bath influence functional takes the form

$$\mathcal{L}(\mathbf{s}) = \sum_{q \in \mathcal{Q}_m} \mathcal{L}_q(\mathbf{s}), \quad (29)$$

where the functional of a given pairing q :

$$\mathcal{L}_q(\mathbf{s}) = \prod_{(j,k) \in q} \langle \tilde{B}(s_k) \tilde{B}(s_j) \rangle_b, \quad (30)$$

corresponding to a particular *diagram* with the coupling lines connecting s_j and s_k on the Keldysh contour (see Fig. 2b). The two-time correlation function of the harmonic bath in the interaction picture can be evaluated semi-analytically prior to the start of the dQMC calculation as

$$\begin{aligned} \langle \tilde{B}(s_k) \tilde{B}(s_j) \rangle_b &= \frac{2}{\pi} \int d\omega J(\omega) \times \\ &\left[\coth\left(\frac{\beta\omega}{2}\right) \cos\omega(s_k - s_j) - i \sin\omega(s_k - s_j) \right]. \end{aligned} \quad (31)$$

In practice, an m -time path configuration includes $(m - 1)!!$ diagrams, and computing each diagram requires $m/2$ evaluations of the bath correlation function. Thus, calculating an m -time correlation function requires a total of $(m - 1)!! (m/2)$ function evaluation, which approaches $\frac{m}{\sqrt{2}} (m/e)^{m/2}$ in the large m limit. This rapidly becomes a bottleneck for high perturbation order. However, rather than explicitly summing over all diagrams in a configuration, it is possible to sum over the pairings as defined in Eq. (29) within the Monte Carlo procedure, thus effectively removing this scaling issue at the cost of an overall increase in the sign problem. In practice, this should only be done if extremely high orders are needed.

B. Restricted propagators and observables

To facilitate our discussion of the inchworm algorithm, we now define *restricted propagators* on contour subintervals. Propagators are defined with respect to particular physical observables. The *bare* restricted propagator $G_{\alpha\beta}^{(0)}(s_f, s_i)$ is defined as follows. When the subinterval $[s_i, s_f]$ is on a single branch of the contour, such that $s_i^+, s_f^+ < t_{\max}$ or $s_i^-, s_f^- > t_{\max}$, then

$$G_{\alpha\beta}^{(0)}(s_f^\pm, s_i^\pm) = \langle \alpha | e^{-iH_s(s_f^\pm - s_i^\pm)} | \beta \rangle. \quad (32)$$

When the endpoints of the interval are on two different branches, it is defined differently in order to account for the observable at the contour's folding point. In this case the operator associated with the observable is $\sigma_z(t_{\max})$, such that:

$$G_{\alpha\beta}^{(0)}(s_f^-, s_i^+) = \langle \alpha | e^{-iH_s(s_f^- - t_{\max})} \sigma_z e^{-iH_s(t_{\max} - s_i^+)} | \beta \rangle. \quad (33)$$

These bare propagators are designated by thin solid lines in the diagrammatic representation (see Fig. 2a). The *full* restricted propagator from s_i to s_f can be defined in terms of Eqs. (32) and (33) with H_S replaced by H , and is evaluated (by way of the Dyson series) as an integral over configurations

$$G_{\alpha\beta}(s_f, s_i) = \int_{\mathbf{s} \in [s_i, s_f]} d\mathbf{s} \mathcal{G}_{\alpha\beta}(\mathbf{s}). \quad (34)$$

The notation $\mathbf{s} \in [s_i, s_f]$ indicates that the vertex times appearing in the configuration \mathbf{s} are restricted to the interval $[s_i, s_f]$. The influence functional then takes the same general form as Eq. (25)

$$\mathcal{G}_{\alpha\beta}(\mathbf{s}) = (-1)^n i^m \mathcal{U}'_{\alpha\beta}(\mathbf{s}) \mathcal{L}(\mathbf{s}), \quad (35)$$

namely it is composed of system and bath parts, $\mathcal{U}'_{\alpha\beta}(\mathbf{s})$ and $\mathcal{L}(\mathbf{s})$. The bath influence functional is identical to the one given by Eqs. (29) and (30), and the system influence functional will be discussed immediately below.

The system influence functional, like the bare propagator, takes on different forms for intervals on a single branch as compared to across branches. For a single branch interval, it is

$$\begin{aligned} \mathcal{U}'_{\alpha\beta}(\mathbf{s} \in [s_i^\pm, s_f^\pm]) &= \\ \langle \alpha | e^{-iH_s s_f^\pm} \tilde{\sigma}_z(s_n^\pm) \cdots \tilde{\sigma}_z(s_1^\pm) e^{iH_s s_i^\pm} | \beta \rangle, \end{aligned} \quad (36)$$

while for a cross-branch interval it becomes

$$\begin{aligned} \mathcal{U}'_{\alpha\beta}(\mathbf{s} \in [s_i^+, s_f^-]) &= \\ \langle \alpha | e^{-iH_s s_f^-} \tilde{\sigma}_z(s_m^-) \cdots \tilde{\sigma}_z(s_{n+1}^-) \times \\ \tilde{\sigma}_z(t) \tilde{\sigma}_z(s_n^+) \cdots \tilde{\sigma}_z(s_1^+) e^{iH_s s_i^+} | \beta \rangle. \end{aligned} \quad (37)$$

Note that if $s_i^+ = s_f^+$ or $s_i^- = s_f^-$, with both times on the same branch, the restricted propagator is trivially equal to $G^{(0)}(s_f, s_f) = G(s_f, s_f) = 1$. However, if $s_i^+ = s_f^-$, with the times appearing on opposite branches, $G_{\alpha\beta}(s_f^-, s_i^+)$ becomes the expectation value of the observable given that the system density matrix was initially in the state $|\beta\rangle \langle \alpha|$:

$$G_{\alpha\beta}(s_f^-, s_i^+) = \langle \langle \alpha | \sigma_z(t - s_f) | \beta \rangle \rangle_b. \quad (38)$$

In terms of diagrams, the full restricted propagator is represented by a thick segment (see Fig. 2a).

C. Inchworm algorithm

Suppose that the full set of restricted propagators $G_{\alpha\beta}(s_k, s_j)$ for all $s_i < s_j, s_k < s_\uparrow$ is known, and one wants to evaluate a restricted propagator over a longer interval $[s_i, s_f]$, with $s_f > s_\uparrow$. It is possible to define an *extended* propagator for the interval $[s_i, s_f]$ by appending the bare propagator to the full propagator:

$$\bar{G}(s_k, s_j) = \begin{cases} G^{(0)}(s_k, s_j) & s_j, s_k > s_\uparrow, \\ G(s_k, s_j) & s_j, s_k < s_\uparrow, \\ G^{(0)}(s_k, s_\uparrow) G(s_\uparrow, s_j) & s_j < s_\uparrow < s_k. \end{cases} \quad (39)$$

Since the contributions of all configurations $\mathbf{s} \in [s_i, s_\uparrow]$ are included in the extended propagator, it is in fact only necessary to sum over configurations in which at least one vertex is contained in the interval $[s_\uparrow, s_f]$. The propagator over the entire interval $[s_i, s_f]$ can be constructed as a path integral over configurations

$$G(s_f, s_i) = \int_{\mathbf{s} \in [s_i, s_f]} d\mathbf{s} \bar{\mathcal{G}}_{\alpha\beta}(\mathbf{s}). \quad (40)$$

The influence functional $\bar{\mathcal{G}}_{\alpha\beta}$ is defined in terms of extended propagators and a modified bath influence functional. It takes the form

$$\bar{\mathcal{G}}(\mathbf{s}) = \bar{G}(s_f, s_m) \cdots \bar{G}(s_2, s_1) \bar{G}(s_1, s_i) \times \sum_{q \in \mathcal{Q}'_m} \mathcal{L}_q(\mathbf{s}). \quad (41)$$

The bath influence functional $\sum_{q \in \mathcal{Q}'_m} \mathcal{L}_q(\mathbf{s})$ is similar to that of Eq. (28), but summation is only carried out over $\mathcal{Q}'_m \subseteq \mathcal{Q}_m$, a subset of the pairings including only *inchworm proper* pairings.

To define inchworm propriety, we first define two pairs to be *connected* if their interaction lines, which are drawn between the members of each pair, cross each other. As connectedness is clearly an equivalence relation, any pairing can be partitioned into disjoint sets of connected pairs, called “clusters”. A pairing or diagram is inchworm proper if this procedure does not generate a cluster with all of its vertices contained in $[s_i, s_\uparrow]$. Put differently, to check whether a particular diagram is inchworm proper one should cluster together sets of interaction lines which cross each other. If and only if every cluster includes at least one line with an endpoint in $[s_\uparrow, s_f]$ is the diagram inchworm proper. This is illustrated in Fig. 2, where two examples of improper diagrams are crossed out.

It is straightforward to prove that any diagram in the bare expansion is accounted for once and only once within the inchworm scheme; therefore, it is formally exact. *However, every inchworm diagram contains an infinite number of bare diagrams, making the expansion substantially more efficient than the bare one.*

This method will be referred to as the System–Bath Coupling Inchworm (SBCI) approach in the companion paper.

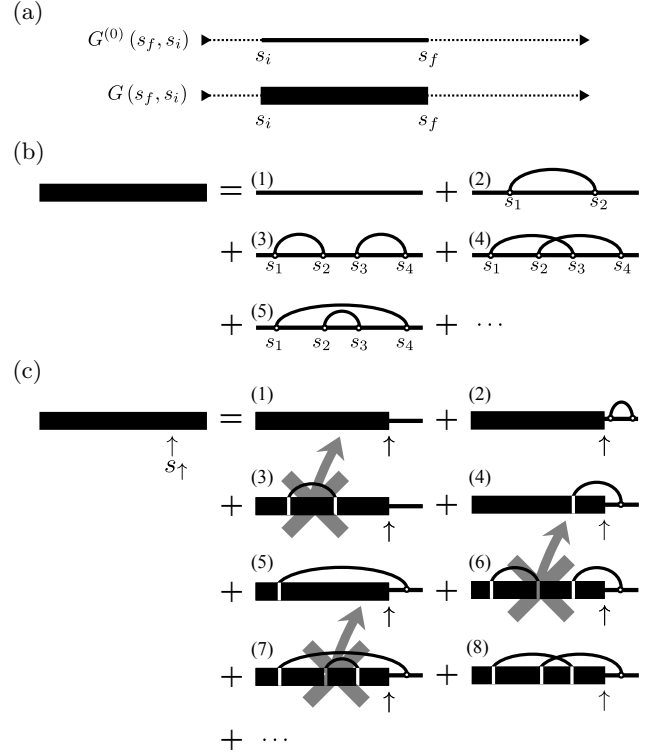


Figure 2. (a) Diagrammatic representation of the bare restricted propagator $G^{(0)}$ (thin solid line) and the full restricted propagator G (thick solid line) of the subinterval $[s_i, s_f]$ on an unfolded Keldysh contour. (b) The bare dQMC expression for the system–bath coupling expansion. The arched curves connecting pairs of vertices within each configuration describe the coupling interaction. Diagram (b.1) is the zeroth order contribution. Diagram (b.2) is the diagram associated with a given 2nd order configuration (s_1, s_2) . Diagrams (b.3)–(b.5) are three diagrams (corresponding to three possible pairings of \mathcal{Q}_4) associated with a 4th order configuration (s_1, s_2, s_3, s_4) . (c) The inchworm algorithm in the system–bath coupling expansion. All the full restricted propagators are assumed to be known for any subinterval to the left of the s_\uparrow time. Diagram (c.1) is the zeroth order inchworm diagram. Diagram (c.2), (c.4) and (c.5) are all inchworm proper 2nd order diagrams. Diagrams (c.3) is an inchworm improper diagram that is included in diagram (c.1). Diagrams (c.6)–(c.8) are associated with the same 4th order configuration. Diagrams (c.6) and (c.7) are included in diagrams (c.4) and (c.5), respectively and only diagram (c.8) is inchworm proper.

IV. DIABATIC COUPLING EXPANSION

A. Polaron transformation

We now consider an expansion in terms of the diabatic coupling $H' = \Delta\sigma_x$, i.e. the spin-flip interaction. Analogous approaches for the Anderson–Holstein model have been very successful in certain regimes.^{21,57–59} The unperturbed Hamiltonian is in this case $H_0 = H_b + \sigma_z(\epsilon + \sum_k c_k x_k)$. Since H_0 commutes with σ_z , its eigenstates maintain the spin quantum number $\sigma = \pm 1$, which

partitions them into two subspaces. Within each subspace the Hamiltonian is easily diagonalized by a polaron transformation. The effective Hamiltonian for the $\sigma = +1$ and $\sigma = -1$ subspaces, respectively, is

$$H_\sigma = H_b + \sigma \left(\epsilon + \sum_\ell c_\ell x_\ell \right). \quad (42)$$

We apply the (canonical) transformation

$$\mathcal{B}_\sigma H_\sigma \mathcal{B}_\sigma^\dagger = H_b + \sigma \epsilon - \sum_\ell \frac{c_\ell^2}{\omega_\ell^2}, \quad (43)$$

where

$$\mathcal{B}_\sigma = e^{\theta_\sigma}, \quad (44)$$

$$\theta_\sigma = \sigma \sum_\ell \frac{c_\ell}{\omega_\ell^{3/2}} (b_\ell^\dagger - b_\ell). \quad (45)$$

Since $\theta_+ = -\theta_-$, it is convenient to write $\mathcal{B}_\sigma^\dagger = \mathcal{B}_{\bar{\sigma}}$. We also define $\epsilon_\sigma = \sigma \epsilon - \sum_\ell \frac{c_\ell^2}{\omega_\ell^2}$. With these definitions, the unperturbed propagator can be written in the form

$$e^{-iH_0 t} = \sum_{\sigma=\pm} e^{-i\epsilon_\sigma t} \mathcal{B}_{\bar{\sigma}} e^{-iH_b t} \mathcal{B}_\sigma |\sigma\rangle \langle \sigma|. \quad (46)$$

In this form the interaction picture time evolution will turn out to be very easy to evaluate, as discussed below.

The natural initial condition for the expansion in the diabatic coupling is $\rho_b = \exp[-\beta H_\pm]$, and using one of these two choices simplifies the expressions substantially. However, in order to allow for rigorous comparison with the system-bath coupling expansion, we choose to start from a state described by $\rho_b = \exp[-\beta H_b]$. Unfortunately, this introduces additional complications in the expressions given below, and we will comment on this as we proceed. The choice of initial condition does not otherwise impact the formalism.

B. Bare dQMC

To obtain a dQMC algorithm for the expectation value of $O = \hat{\sigma}_z$, we must write the contribution $\mathcal{O}(\mathbf{s})$ of a configuration \mathbf{s} in the form of Eq. 12. In the interaction picture, $\tilde{\sigma}_x(s) = e^{iH_0 s} \sigma_x e^{-iH_0 s}$, we can write

$$\mathcal{O}(\mathbf{s}) = (-1)^n i^m \Delta^m \left\langle \tilde{\sigma}_x(s_m) \cdots \tilde{\sigma}_x(s_{n+1}) \times \tilde{\sigma}_z(t) \tilde{\sigma}_x(s_n) \cdots \tilde{\sigma}_x(s_1) \right\rangle. \quad (47)$$

We designate the state between $[s_k, s_{k+1}]$ as σ_{k+1} for $k \in \{0, \dots, m-1\}$, with $s_0 \equiv 0^+$ and $s_{m+1} \equiv 0^-$. The observable σ_z at the tip of the contour does not change the state, while every application of σ_x flips the state from σ to $\bar{\sigma}$. Since the initial condition of the spin is

specified $\rho_s = |1\rangle \langle 1| = |+\rangle \langle +|$, we have $\sigma_1 = \sigma_{m+1} = +$. The contribution $\mathcal{O}(\mathbf{s})$ of a configuration \mathbf{s} to the expectation value of $O = \hat{\sigma}_z$ can then be expressed as a product of a system influence functional $\Phi(\mathbf{s})$ and a bath influence functional $\mathcal{J}(\mathbf{s})$:

$$\mathcal{O}(\mathbf{s}) = (-1)^n i^m \Delta^m \Phi(\mathbf{s}) \mathcal{J}(\mathbf{s}). \quad (48)$$

The system functional $\Phi(\mathbf{s})$ handles the influence of propagation within the system,

$$\Phi(\mathbf{s}) = \langle +1 | \sigma_x^{n'} \sigma_z \sigma_x^n | +1 \rangle \times \exp \left[-i \sum_{k=1}^{m+1} \epsilon_{\sigma_k} (s_k - s_{k-1}) \right], \quad (49)$$

whiles the bath functional $\mathcal{J}(\mathbf{s})$ is a multi-time correlation function of bath operators

$$\mathcal{J}(\mathbf{s}) = \left\langle \tilde{\mathcal{B}}_-(s_{m+1}) \prod_{k=1}^m \tilde{\mathcal{B}}_{\sigma_k}^2(s_k) \tilde{\mathcal{B}}_+(s_0) \right\rangle_b. \quad (50)$$

Here $\langle \cdot \rangle_b = \text{Tr}_b \{ \rho_b \cdot \}$ and ρ_b is the initial bath density matrix. The first and last factors are induced by the initial condition. By a generalized Wick's theorem for polaron shift operator (see Appendix A), we can write $\mathcal{J}(\mathbf{s})$ as a product of two-time correlation functions,

$$\mathcal{J}(\mathbf{s}) = \frac{\prod_{(j,k) \in \mathcal{C}_{m+2}^{\text{odd}}} C(s_k, s_j)^{r_k r_j}}{\prod_{(j,k) \in \mathcal{C}_{m+2}^{\text{even}}} C(s_k, s_j)^{r_k r_j}}. \quad (51)$$

where $r_i = 1$ if $i = 1, m+1$, otherwise $r_i = 2$. The fact that the powers in the numerator and denominator may differ arises from the initial condition. Here we have defined

$$\mathcal{C}_{m+2}^{\text{even}} = \{ (j, k) \in \mathcal{C}_{m+2} \mid |k - j| \text{ even} \}, \quad (52)$$

and

$$\mathcal{C}_{m+2}^{\text{odd}} = \{ (j, k) \in \mathcal{C}_{m+2} \mid |k - j| \text{ odd} \}. \quad (53)$$

which are subsets of all possible pairings of $m+2$ elements. The pairings of m elements, \mathcal{C}_m , denotes the set of all ordered tuples composed of different integers between 0 and $m-1$. For example,

$$\mathcal{C}_2^{\text{odd}} = \{(0, 1)\}, \quad \mathcal{C}_2^{\text{even}} = \{\},$$

where $\{\}$ denotes the empty set and

$$\mathcal{C}_4^{\text{odd}} = \{(0, 1), (1, 2), (2, 3), (0, 3)\}, \\ \mathcal{C}_4^{\text{even}} = \{(0, 2), (1, 3)\}.$$

The correlation function $C(s_k, s_j)$ is one of the expressions complicated by the initial condition, and is given by

$$C(s_k, s_j) = \left\langle \tilde{\mathcal{B}}_-(s_k) \tilde{\mathcal{B}}_+(s_j) \right\rangle_b \quad (54)$$

In general, we can write the two-time correlation function of the polaron shift operator as (see Appendix. (A))

$$C(s_k, s_j) = e^{-Q_2(s) - iQ_1(s)}, \quad (55)$$

with

$$Q_1(s) = \frac{2}{\pi} \int d\omega \frac{J(\omega)}{\omega^2} \sin \omega s, \quad (56)$$

and

$$Q_2(s) = \frac{2}{\pi} \int d\omega \frac{J(\omega)}{\omega^2} \coth\left(\frac{\beta\omega}{2}\right) (1 - \cos \omega s). \quad (57)$$

In the diagrammatic representation shown in Fig. 3, the two-time correlation function is represented by dashed lines. There exists an extra set of lines due to the initial condition, which connect every vertex to the edges of the diagram. To avoid overcrowding the diagram with information, these are not shown. A dashed line above the contour describes a contribution to the numerator, while one under the contour describes one associated with the denominator. Each vertex is connected by such interaction lines to every other vertex in the configuration, and since only one way to do this exists, each configuration generates exactly one diagram. The bare Monte Carlo implementation based on this expansion is illustrated in Fig. 3b.

C. Inchworm algorithm

The process of formulating an inchworm expansion is analogous to that of Sec. IIIC, but with the diagrammatic structure of the diabatic coupling expansion. Inchworm proper and improper diagrams are illustrated in Fig. 3c. The main difference is that whereas diagrams in the system-bath coupling expansion include interaction lines only between vertices paired within a particular pairing, the diabatic coupling expansion includes an interaction line between every two vertices. Therefore, there is only one “cluster” of vertices in every diagram, and that diagram is required to have at least one vertex in $[t_\uparrow, t_f]$. The only diagram not containing such a cluster is the order zero diagram (shown as (1) in Fig. 3c). This is also the only diagram containing an infinite number of bare diagrams: each diagram containing a cluster is completely identical to the one and only bare diagram that it represents.

The main advantages of the inchworm algorithm are therefore lost in the direct diabatic coupling scheme described here, and indeed we have verified that upon implementation of such an algorithm an exponential dynamical sign problem appears (not shown). However, in the remainder of this paper, this problem is circumvented by transforming the expansion to a cumulant form. From this perspective, a very useful inchworm algorithm then emerges.

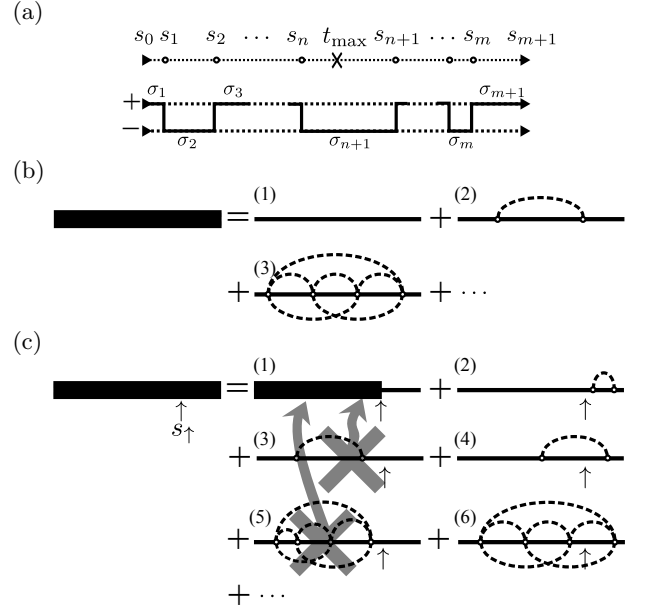


Figure 3. (a) A configuration including $s_0 = s_i$ and $s_{m+1} = s_f$ for the diabatic coupling expansion. The state of the system flips at every s_i . (b) Diagrams appearing in bare dQMC. The dashed curve (12) indicates an interaction line in either the numerator (above the contour) or the denominator (below it). Only one diagram corresponds to each configuration. (c) The naive inchworm scheme. Diagrams with no vertices after s_\uparrow (such as (c.3) and (c.5)) are contained in the zeroth order term (c.1) and need not be summed. Other diagrams, such as (c.4) and (c.6), are analogous to those of the bare dQMC.

V. DIABATIC COUPLING CUMULANT INCHWORM (DCCI) EXPANSION

As noted in Sec. IV, the diabatic coupling expansion in its direct Keldysh formulation has a peculiar diagrammatic structure in which each interaction vertex is directly connected to every other vertex. As such, this expansion does not significantly benefit from the inchworm algorithm, which relies on the ability to cut diagrams into weakly-connected subgraphs. We now show that by reformulating the diabatic coupling expansion in cumulant form, one obtains a formalism which is much more amenable to inchworm dQMC. The cumulant formalism has the additional advantage of being written in physical (rather than contour) time, such that in the absence of a sign problem the computation scales linearly with time, as will be demonstrated in the companion paper.

Since cumulants are most conveniently defined in terms of moments, the moment form of the expansion will first be presented. Cumulants and the cumulant inchworm algorithm will then be presented.

A. Moments

Consider the evaluation of the dynamics of an observable O in terms of its *moments*, $\mu_m(\tau_1, \dots, \tau_m)$. Given that we have Eq. (10), such that $\langle O(t) \rangle = \int d\mathbf{s} \mathcal{O}(\mathbf{s})$, the observable can be written in terms of a moment expansion

$$\int d\mathbf{s} \mathcal{O}(\mathbf{s}) = \sum_{m=0}^{\infty} \int d\boldsymbol{\tau} \mu_m(\tau_1, \tau_2, \dots, \tau_m). \quad (58)$$

While the integration $\int d\mathbf{s}$ is performed over contour time, the integration $\int d\boldsymbol{\tau}$ is performed over physical times $\tau_1 > \tau_2 > \dots > \tau_m$, such that

$$\int d\boldsymbol{\tau} = \int_0^t d\tau_1 \int_0^{\tau_1} d\tau_2 \dots \int_0^{\tau_{m-1}} d\tau_m. \quad (59)$$

An m^{th} -order moment $\mu_m(\tau_1, \tau_2, \dots, \tau_m)$ is defined as

$$\mu_m(\tau_1, \dots, \tau_m) = \sum_{\alpha_i \in \{+, -\}} \mathcal{O}(\mathcal{T}_c[\tau_1^{\alpha_1}, \dots, \tau_m^{\alpha_m}]), \quad (60)$$

where \mathcal{T}_c indicates contour time ordering and the $\alpha_i = \pm$ are the Keldysh branch indices. The moments are defined as functions of a set of real times, and the Keldysh branch indices are summed over. This is equivalent to simultaneously collecting the contributions from entire classes of path configurations associated with the real times, τ_1, \dots, τ_m , as illustrated diagrammatically in Fig. 4a. Notably, it is exponentially expensive as a function of the order m to evaluate moments in terms of diagrams, as an m^{th} order moment is the sum of 2^m diagrams.

For the population operator $O = \sigma_z$ in the diabatic coupling expansion, the 0^{th} order moment is $\mu_0 = 1$ and odd moments vanish, $\mu_{2n+1} = 0$. The expectation value of σ_z can therefore be written in terms of the even moments

$$\begin{aligned} \langle \sigma_z(t) \rangle &= 1 + \int_0^t d\tau_1 \int_0^{\tau_1} d\tau_2 \mu_2(\tau_1, \tau_2) \\ &+ \int_0^t d\tau_1 \int_0^{\tau_1} d\tau_2 \int_0^{\tau_2} d\tau_3 \int_0^{\tau_3} d\tau_4 \quad (61) \\ &\times \mu_4(\tau_1, \tau_2, \tau_3, \tau_4) \\ &+ \dots \end{aligned}$$

With the initial density matrix $|1\rangle\langle 1| e^{-\beta H_b}$ specified earlier, the second population moment simplifies to⁵³

$$\mu_2(\tau_1, \tau_2) = -4\Delta^2 \text{Re} \left\{ e^{2i\epsilon(\tau_1 - \tau_2)} \mathcal{J}(0^+, \tau_2^+, \tau_1^+, 0^-) \right\}, \quad (62)$$

and the fourth moment to

$$\begin{aligned} \mu_4(\tau_1, \tau_2, \tau_3, \tau_4) &= 4\Delta^2 \times \text{Re} \left\{ \right. \\ &e^{2i\epsilon(\tau_1 - \tau_2 + \tau_3 - \tau_4)} \mathcal{J}(0^+, \tau_4^+, \tau_3^+, \tau_2^+, \tau_1^+, 0^-) + \\ &e^{2i\epsilon(\tau_1 - \tau_2 - \tau_3 + \tau_4)} \mathcal{J}(0^+, \tau_4^+, \tau_3^+, \tau_1^-, \tau_2^-, 0^-) + \quad (63) \\ &e^{-2i\epsilon(\tau_1 - \tau_2 - \tau_3 + \tau_4)} \mathcal{J}(0^+, \tau_4^+, \tau_2^+, \tau_1^-, \tau_3^-, 0^-) + \\ &\left. e^{-2i\epsilon(\tau_1 - \tau_2 + \tau_3 - \tau_4)} \mathcal{J}(0^+, \tau_3^+, \tau_2^+, \tau_1^+, \tau_4^-, 0^-) \right\}. \end{aligned}$$

Evaluating the moments within dQMC is therefore an alternative scheme for calculating dynamics. While linear in time (rather than quadratic, like the Keldysh formalism which involves two times), this expansion involves an additional exponential cost in the diagram order, due to the summation over the Keldysh indices. However, bare moment expansions typically converge very slowly if at all, and hold no real advantage over a direct calculation (though they may be of help with sign problems in certain cases⁶⁰). It is therefore often advantageous to resum moments into cumulants. It turns out that a relationship exists between cumulant resummation and the inchworm algorithm, and this will be shown below.

B. Cumulants

Moment expansions can be immediately resummed into cumulant expansions in several ways.^{50,53} For the present purpose, it is advantageous to choose the chronological ordering prescription (COP) cumulant expansion,⁵³ which yields the time-nonlocal equation of motion

$$\begin{aligned} \frac{d\langle \sigma_z(t) \rangle}{dt} &= \sum_{m=2}^{\infty} \int_0^t d\tau_1 \int_0^{\tau_1} d\tau_2 \dots \int_0^{\tau_{m-2}} d\tau_{m-1} \quad (64) \\ &\times \gamma_m(t, \tau_1, \dots, \tau_{m-1}) \langle \sigma_z(\tau_{m-1}) \rangle. \end{aligned}$$

An advantage from the inchworm perspective is immediately apparent: the expression depends on the population at shorter times, such that previously calculated properties can perhaps be reused. The m -th order COP cumulant $\gamma_m(t, \tau_1, \dots, \tau_{m-1})$ can be obtained by plugging Eq. (61) into both sides of Eq. (64) and equating terms of equal order. For example,

$$\gamma_2(\tau_1, \tau_2) = \mu_2(\tau_1, \tau_2), \quad (65)$$

$$\gamma_4(\tau_1, \tau_2, \tau_3, \tau_4) = \mu_4(\tau_1, \tau_2, \tau_3, \tau_4) - \mu_2(\tau_1, \tau_2) \mu_2(\tau_3, \tau_4), \quad (66)$$

and $\gamma_{2n-1} = 0$. A general m -th order cumulant, γ_m , can be obtained recursively:

$$\begin{aligned} \gamma_m(\tau_1, \dots, \tau_m) &= \sum_{p \in \mathcal{P}_m} -(-1)^{|p|} \times \\ &\prod_{(i_1, i_2, \dots, i_{2n}) \in p} \mu_{2n}(\tau_{i_1}, \tau_{i_2}, \dots, \tau_{i_{2n}}). \quad (67) \end{aligned}$$

The set \mathcal{P}_m describes all possible ways of partitioning a sequence of integers $1, 2, \dots, m$ into subsequences of adjacent numbers, each having an even number elements. Each partition $p \in \mathcal{P}_m$ can be represented by a set of ordered tuples $(i_1, i_2, \dots, i_{2n})$ corresponding to one subsequence, and $|p|$ is the number of subsequences within the partition. For instance,

$$\mathcal{P}_2 = \{\{(1, 2)\}\},$$

$$\mathcal{P}_4 = \{\{(1, 2, 3, 4)\}, \{(1, 2), (3, 4)\}\},$$

$$\mathcal{P}_6 = \{\{(1, 2, 3, 4, 5, 6)\}, \{(1, 2), (3, 4, 5, 6)\}, \\ \{(1, 2, 3, 4), (5, 6)\}, \{(1, 2), (3, 4), (5, 6)\}\}.$$

The diagrammatic description of COP cumulants in terms of moments is shown in Fig. 4b. A cumulant of any given order can be expressed in terms of moments up to and including the same order.

C. Naive inchworm algorithm

The dynamics of $\langle \sigma_z(t) \rangle$ within the COP cumulant expansion can be evaluated by dQMC. To simplify the notation, it is convenient to redefine the times $t, \tau_1, \dots, \tau_{m-1}$ as $\tau_1, \tau_2, \dots, \tau_m$, respectively; these obey the physical time ordering $\tau_1 > \dots > \tau_m$. As before, the times will be indicated by the vector quantity $\boldsymbol{\tau}$ when possible. By carrying out the integration $\int_0^t d\tau_1$ on both sides of Eq. (64), an expression for $\langle \sigma_z(t) \rangle$ in terms of itself is obtained:

$$\langle \sigma_z(t) \rangle = 1 + \int_0^t d\boldsymbol{\tau} \mathcal{K}(\boldsymbol{\tau}), \quad (68)$$

$$\mathcal{K}(\boldsymbol{\tau}) = \gamma_m(\tau_1, \dots, \tau_m) \langle \sigma_z(\tau_m) \rangle. \quad (69)$$

Since $\gamma_{2n-1} = 0$, the path integration $\int_0^t d\boldsymbol{\tau}$ can be explicitly written as

$$\int_0^t d\boldsymbol{\tau} = \sum_{m \in \text{even}, \geq 2} \int_0^t d\tau_1 \int_0^{\tau_1} d\tau_2 \dots \int_0^{\tau_{m-1}} d\tau_m. \quad (70)$$

Since the functional $\mathcal{K}(\boldsymbol{\tau})$ depends on $\langle \sigma_z(t_m) \rangle$, the observable is evaluated at the smallest time in the configuration $\boldsymbol{\tau}$. Since this is the quantity being evaluated, it is not known to begin with and there is no bare expansion of the COP type. However, it is straightforward to implement a simple inchworm algorithm: assume $\langle \sigma_z(\tau) \rangle$ is known for all $\tau \in [0, \tau_\uparrow]$. The expectation value at $t > \tau_\uparrow$ can then be expressed as:

$$\langle \sigma_z(t) \rangle = \langle \sigma_z(\tau_\uparrow) \rangle + \int_{\tau_\uparrow}^t d\boldsymbol{\tau} \mathcal{K}(\boldsymbol{\tau}). \quad (71)$$

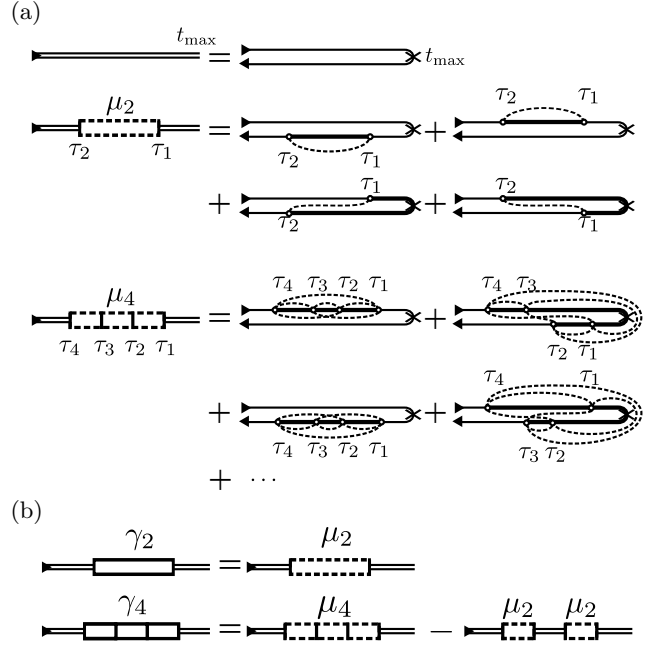


Figure 4. (a) The real-time coordinate is represented by the thin double lines. The bare double line segment $[0, t_{\max}]$ corresponds to the bare propagator in the diabatic expansion on the Keldysh contour folded at t_{\max} . A m^{th} order moment of a real time configuration $(\tau_1, \tau_2, \dots, \tau_m)$ is illustrated as a dashed-edged box from τ_1 to τ_m with solid vertical ticks at each configuration time. There are 4 distinct diagrams on the Keldysh contour associated with the 2nd moment $\mu_2(\tau_1, \tau_2)$: $\mathbf{s} = (\tau_1^-, \tau_2^-), (\tau_2^+, \tau_1^+), (\tau_1^+, \tau_2^-), (\tau_2^-, \tau_1^-)$. These diagrams are plotted by connecting the vertices with the diabatic interaction lines as in Fig. (3). The 4th moment contains 2^4 diagrams on the contour. Here, we demonstrate only 4 example diagrams. (b) The COP cumulants of a real-time configuration $(\tau_1, \tau_2, \dots, \tau_m)$ are illustrated as a solid-edged box with vertical ticks at each configuration time. Here, we show the diagrammatic representation of Eq. (65) and (66), which illustrate the 2nd and 4th cumulants in terms of the moments.

Here $\int_{\tau_\uparrow}^t d\boldsymbol{\tau}$ represents the path integral

$$\int_{\tau_\uparrow}^t d\boldsymbol{\tau} = \sum_{m=2}^{\infty} \int_{\tau_\uparrow}^t d\tau_1 \int_0^{\tau_1} d\tau_2 \dots \int_0^{\tau_{m-1}} d\tau_m, \quad (72)$$

which describes integration over the configuration subspace for which at least one τ_1 is within the interval $[\tau_\uparrow, t]$. This defines a formally exact inchworm step, which appears to leverage knowledge of $\langle \sigma_z(\tau) \rangle$ for times up to τ_\uparrow in order to obtain the same observable for the final time t . Examples of diagrams appearing in this expansion are shown in Fig. 5. Diagrams in which the rightmost time index is to the left of τ_\uparrow (crossed out in the figure) are included in the 0th order contribution (diagram (1) in Fig. 5) and need not be summed.

Unfortunately, the inchworm step we have just described cannot be implemented as it stands, and has been introduced chiefly for didactic purposes. This is because it includes contributions where $\langle \sigma_z(\tau) \rangle$ is needed at time

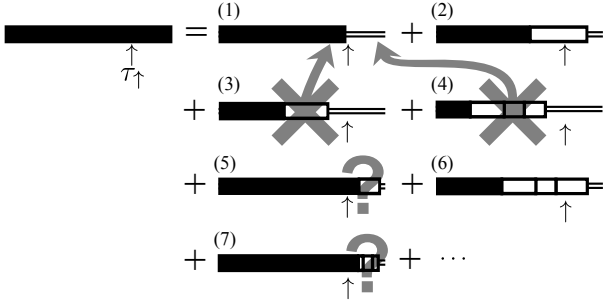


Figure 5. Diagrammatic representation of the naive prescription of the inchworm algorithm, Eq. (71). The solid-edged boxes with vertical ticks are the COP cumulants as shown in Fig. (4). The τ_{\uparrow} is indicated as the \uparrow on the physical time coordinate. Each configuration corresponds to one single diagram. Diagrams (3) and (4) have all cumulant boxes lying in the known region (to the left of \uparrow) and are considered been included in diagram (1) for this inchworm step. The cumulant boxes in diagrams (2) and (6) straddle the τ_{\uparrow} time and their contribution can be calculated by Eq. (69). Diagrams (5) and (7) have all cumulant boxes located to the right of the \uparrow , are unknown for this inchworm step in the naive version.

argument $\tau > \tau_{\uparrow}$. Two examples are overlaid with a question mark in Fig. 5. Such contributions are unknown and must be dropped from the expansion, leading to an error the magnitude of which can be shown to be linear in $\Delta t = t - \tau_{\uparrow}$. In practice, this makes convergence of the algorithm to the exact result (by progressively reducing the size of the inching time step Δt) very hard to achieve. However, as the next subsection shows, this issue can be overcome by taking a closer look at the structure of the diagrams.

D. Cumulant inchworm algorithm

It is now necessary to solve the problem raised in the previous subsection, namely the fact that one is unable to evaluate diagrams from configurations having $\tau_m > \tau_{\uparrow}$ for some m . To do so, it is possible to first *unwind* the resumming done implicitly by the cumulant expansion, then reintroduce it wherever possible. To see how this works, one inserts the functional Eqs. (68) and (69). This gives

$$\langle \sigma_z(t) \rangle = 1 + \int_0^t d\tau \gamma_m(\tau) + \int_0^t d\tau \gamma_m(\tau) \int_0^{\tau_m} d\tau' \mathcal{K}(\tau'), \quad (73)$$

and we sample an additional configuration τ' for the integration $\int_0^{\tau_m} d\tau'$. This can be iterated any number of times, generating an expansion in terms of multiple cumulants, with the population pushed to increasingly high-order terms. Examples of terms appearing in this unwound cumulant expansion are shown in Fig. 6a. The

term “wound / wind” is used to distinguish this procedure from “dressing / dress” used in the context of Dyson equations, and in particular to distinguish “unwound” from “bare.”

The unwound expansion can be written as

$$\langle \sigma_z(t) \rangle = 1 + \int d\tau \Gamma(\tau), \quad (74)$$

where the functional Γ depends only on the COP cumulants. At a general (even) order m , Γ contains terms of various partitions \mathcal{P}_m , as introduced in Sec. VB:

$$\Gamma(\tau_1, \dots, \tau_m) = \sum_{p \in \mathcal{P}_m} \prod_{(i_1, i_2, \dots, i_{2n}) \in p} \gamma_{2n}(\tau_{i_1}, \tau_{i_2}, \dots, \tau_{i_{2n}}). \quad (75)$$

For instance, the lowest order functional ($m = 2$) is simply

$$\Gamma(\tau_1, \tau_2) = \gamma_2(\tau_1, \tau_2), \quad (76)$$

while that with $m = 4$ contains two terms originating from the iteration procedure:

$$\Gamma(\tau_1, \tau_2, \tau_3, \tau_4) = \gamma_4(\tau_1, \tau_2, \tau_3, \tau_4) + \gamma_2(\tau_1, \tau_2) \gamma_2(\tau_3, \tau_4). \quad (77)$$

Unlike the original bare expansion in diabatic coupling, each configuration now generates multiple diagrams (corresponding to partitions). For instance, as we show in Fig. 6a, a 4th order configuration generates 2 diagrams, (a.3) and (a.4), and a 6th order configuration generates 4 diagrams, (a.5)–(a.8). We note briefly that it is easy to show that the unwound expansion corresponds exactly to the moment expansion, in the sense that $\Gamma_i = \mu_i$. However, the advantages of the unwound representation will immediately become apparent.

The unwinding completely removes the dependence on the population $\langle \sigma_z(\tau) \rangle$, but does so at the cost that the resummation properties of the COP expansion are lost. We now *partially rewind* the series wherever this does not interfere with the assumptions of the inchworm step, in particular the fact that we only have access to populations for $\tau < \tau_{\uparrow}$. The inchworm step is performed by stochastically sampling configurations $\tau = (\tau_1, \dots, \tau_m) \in [0, t]$, as before

$$\langle \sigma_z(t) \rangle = \langle \sigma_z(\tau_{\uparrow}) \rangle + \int_{\tau_{\uparrow}}^t d\tau \mathcal{K}'(\tau). \quad (78)$$

For each configuration, one sums only diagrams stemming from a *proper* subset of the partitions, $\mathcal{P}'_m \subseteq \mathcal{P}_m$, obtained by excluding partitions with subsequences (parts) having all times in $[0, \tau_{\uparrow}]$. With this, we define

$$\Gamma'(\tau) = \sum_{p \in \mathcal{P}'_m} \prod_{(i_1, i_2, \dots, i_{2n}) \in p} \gamma_{2n}(\tau_{i_1}, \tau_{i_2}, \dots, \tau_{i_{2n}}), \quad (79)$$

such that the functional to be summed is

$$\mathcal{K}'(\tau) = \begin{cases} \Gamma'(\tau) \langle \sigma_z(\tau_m) \rangle & \text{if } \tau_m < \tau_{\uparrow}, \\ \Gamma'(\tau) \langle \sigma_z(\tau_{\uparrow}) \rangle & \text{if } \tau_m > \tau_{\uparrow}. \end{cases} \quad (80)$$

The diagrammatic representation of this cumulant inchworm expansion is illustrated in Fig. 6b, where three examples of improper partitions (diagrams) are crossed out. Note that contribution (b.8) takes into account precisely the kind of diagram missing in the naive inchworm algorithm.

To justify that the cumulant inchworm expansion is formally equivalent to the unwound expansion, it must be shown that the two sets of diagrams generated by respective expansions are identical. To do so, we have to prove that (a) these two sets of diagrams contain each other, in the sense that every unwound diagram in one set is *represented* in the other; and (b), each diagram in one set is mapped to only a *single* diagram in the other set (such that the measure is conserved under summation). We will proceed by example, rather than presenting a formal proof.

To argue point (a), we need to show a containment relationship in both directions. First, any cumulant inchworm diagram generates only diagrams contained in the set of unwound diagrams. This is trivial since the thick solid segment in each cumulant inchworm diagram can be considered an infinite sum of unwound diagrams within that segment. In the reverse direction, any unwound diagram can be found in the set of cumulant inchworm diagrams: given an unwound diagram, one can construct a cumulant inchworm diagram containing it by Eqs. (79) and (80). As an example, we consider the lowest order in Fig. 6b with a 2nd order configuration $\tau = (\tau_1, \tau_2)$. The configuration generates one unwound diagram of the (a.2) type. For the same configuration's cumulant inchworm diagram, three cases are possible: $\tau_1 > \tau_\uparrow > \tau_2$, $\tau_\uparrow > \tau_1 > \tau_2$, and $\tau_1 > \tau_2 > \tau_\uparrow$, which correspond to diagrams (b.2), (b.3), and (b.5), respectively. It is clear that diagram (b.3) is improper and has been included in diagram (b.1). Thus, an unwound diagram of the (a.2) type is contained in (b.2), (b.3), or (b.1) depending on its relationship with τ_\uparrow .

Point (b) requires unique correspondence in both directions. One direction is trivial—each cumulant inchworm diagram can be written as an infinite sum of unique unwound diagrams. In the other direction, we need to show that if there exist two cumulant inchworm diagrams which contain the same unwound diagram, one of these two cumulant inchworm diagrams must be eliminated. The propriety of cumulant inchworm diagrams ensures this uniqueness: consider a 4th-order unwound diagram of type (a.4) with configuration $\tau = (\tau_1, \tau_2, \tau_3, \tau_4)$. If $\tau_1 > \tau_\uparrow > \tau_2$, the unwound diagram could in principle be contained in two (not necessarily proper) cumulant inchworm diagrams, (b.2) and (b.4). Diagram (b.4) is then eliminated by the requirement of propriety. Similarly, if $\tau_2 > \tau_\uparrow > \tau_3$, the unwound diagram could be contained in two cumulant inchworm diagrams, (b.5) and (b.7), but (b.7) is improper and therefore can be eliminated. For other cases, the uniqueness is trivial: there is only one (necessarily proper) cumulant inchworm diagram containing the unwound diagram. For example, if

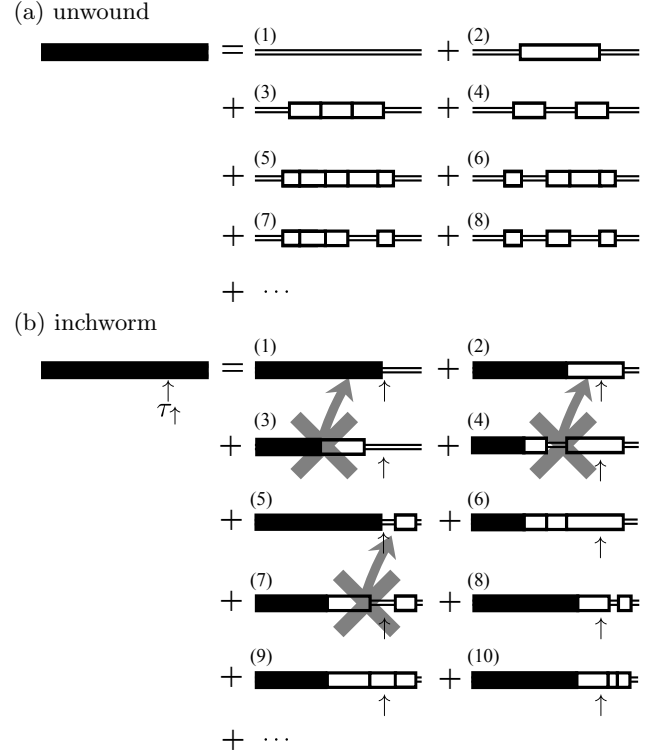


Figure 6. (a) The unwound dQMC expression for the full cumulant expansion. The thick solid lines are the exact dynamics of expectation value and the thin double lines are the unperturbed value 1 within the diabatic expansion. The solid-edged boxes with vertical ticks are the COP cumulants as shown in Fig. (4). Each configuration may yield more than one diagram: 2-time configurations gives one 2nd order diagram (a.2); 4-time configurations yield diagrams (a.3) and (a.4) corresponding to 2 partitions in \mathcal{P}_4 ; 6-time configurations contain diagrams (a.5)–(a.8) corresponding to 4 partitions in \mathcal{P}_6 . (b) The cumulant inchworm algorithm. Any diagram that has a stand alone part (a cumulant box) to the left of the \uparrow has been included in the other diagrams and needs to be neglected in the inchworm step. Diagram (b.3) is included in diagram (b.1); diagram (b.4) is included in diagram (b.2); diagram (b.7) is included in diagram (b.5).

$\tau_3 > \tau_\uparrow > \tau_4$, only diagram (b.8) can contain it.

With points (a) and (b) justified, it is clear that an exact correspondence exists between the cumulant inchworm expansion and the unwound expansion. Every diagram in the cumulant inchworm expansion corresponds to an infinite number of unwound diagrams, and while the expansion does not perform resummation over the entire length of the contour like the system–bath coupling expansion, it also has the distinct advantage of scaling linearly in time. It therefore constitutes a highly efficient method which is complementary to the system–bath coupling inchworm approach.

This method will be referred to as the Diabatic Coupling Cumulant Inchworm (DCCI) approach in the companion paper.

VI. CONCLUSIONS

In this paper we develop two complementary dQMC inchworm approaches for the simulation of exact real-time non-adiabatic dynamics. These approaches are based on generic expansions in either the system–bath coupling or the diabatic coupling, respectively, and thus should be of general utility. For concreteness, as well as to permit benchmarking of the approach, we specialize to the case of the spin–boson model. A discussion of the relative benefits and drawbacks of our approach and detailed comparisons to established exact methods will be presented in the companion paper.

Our first approach is based on a system–bath coupling expansion, analogous to the hybridization expansion in the Anderson model. Indeed the scheme is nearly identical to that employed in original inchworm algorithm formulated for the Anderson impurity model.³⁸ Only the definitions of connectedness and propriety of diagrams differ, due to the differences in the model systems studied. We formally show that proper inchworm diagrams account for any diagram in the bare Monte Carlo expansion once and only once. The major advantages of the SBCI approach are twofold: there are far fewer proper inchworm diagrams than bare diagrams and an infinite number of bare diagrams are resummed in each contribution to the inchworm expansion. However, this advantage comes at a cost, namely one has to calculate two-time restricted propagators and perform a more involved error analysis during inchworm propagation.

The second inchworm approach is based on the diabatic coupling expansion and its cumulant form. Due to the fact that diagrams within the diabatic coupling expansion include an interaction line between every two vertices, the main advantages of the inchworm algorithm are lost if one follows the previous scheme. To circumvent this problem, we introduce a cumulant form of the expansion and propose an alternative inchworm approach, the diabatic coupling cumulant inchworm (DCCI) expansion. The DCCI expansion has the notable advantage that only single-time properties are needed, and the simulation scales linearly in time. Since cumulant forms can also be used in other inchworm expansions (such as the SBCI approach), this property should be of general utility. We also note that since the DCCI and SBCI expansions converge differently in distinct parameter regimes, we expect their combined use to cover much, if not all, of the relevant parameter space.

The formulations of Monte Carlo approaches with suppressed sign errors presented here are quite general. They provide a framework allowing for the simulation of both non-equilibrium and equilibrium observables in general impurity-type problems. Many of these problems are out of reach for existing methods and their exact interrogation remains an open challenge. This work paves the way to explore the scope of the inchworm dQMC methodology in such frontier problems, which will be the subject of future studies.

ACKNOWLEDGMENTS

We would like to thank Eran Rabani and Andrés Montoya-Castillo for discussions. GC and DRR would like to thank Andrew J. Millis and Emanuel Gull for previous collaboration on the inchworm algorithm. DRR acknowledges support from NSF CHE-1464802. GC and HTC acknowledge support from the Raymond and Beverly Sackler Center for Computational Molecular and Materials Science, Tel Aviv University.

Appendix A: Wick's theorem in the diabatic coupling expansion

The multi-time correlation function of polaron shift operators given in Eq. (50) can be written as

$$\mathcal{J}(s) = \left\langle \tilde{\mathcal{B}}_-(s_{m+1}) \tilde{\mathcal{B}}_+^2(s_m) \cdots \tilde{\mathcal{B}}_-^2(s_1) \tilde{\mathcal{B}}_+(s_0) \right\rangle_b. \quad (\text{A1})$$

The explicit form of the polaron shift operator in the interaction picture is given by

$$\tilde{\mathcal{B}}_\sigma(s) = e^{\tilde{\theta}_\sigma(s)}, \quad (\text{A2})$$

$$\tilde{\theta}_\sigma(s) = \sigma \sum_\ell \frac{c_\ell}{\omega_\ell^{3/2}} \left(e^{i\omega_\ell s} b_\ell^\dagger - e^{-i\omega_\ell s} b_\ell \right). \quad (\text{A3})$$

To simplify the notation, we drop the ℓ index for the time being and define $\xi(s) = \frac{c}{\omega^{3/2}} e^{i\omega s}$, such that

$$\tilde{\theta}_\sigma(s) = \sigma \left(\xi(s) b^\dagger - \xi(s)^* b \right). \quad (\text{A4})$$

The arguments of the polaron shift operators product can be combined using the identity

$$e^{vb^\dagger - v^*b} e^{ub^\dagger - u^*b} = e^{(v+u)b^\dagger - (v^*+u^*)b} \times e^{(vu^* - v^*u)/2} \quad (\text{A5})$$

for boson operators b and b^\dagger (as can easily be derived using the Baker–Campbell–Hausdorff formula).

Next, the two-time correlator of polaron shift operators is

$$\begin{aligned} \mathcal{B}_{\sigma'}^{r'}(s') \mathcal{B}_\sigma^r(s) &= \exp \left\{ [\sigma' r' \xi(s') + \sigma r \xi(s)] b^\dagger - \text{c.c.} \right\} \times \\ &\quad \exp \left\{ i \sigma' \sigma r' r \text{Im} [\xi(s') \xi(s)^*] \right\}. \end{aligned} \quad (\text{A6})$$

We note that the boson operator part of the correlator takes the same form as the polaron shift operator and an additional scalar factor (not a boson operator) emerges. Therefore, we can recursively combine the argument using the above identity and find a general expression for the multi-time correlator

$$\begin{aligned} \prod_j \mathcal{B}_{\sigma_j}^{r_j}(s_j) &= \exp \left\{ \sum_j \sigma_j r_j \xi(s_j) b^\dagger - \text{c.c.} \right\} \times \\ &\quad \exp \left\{ i \sum_j \sum_{k < j} \sigma_j \sigma_k r_j r_k \text{Im} [\xi(s_j) \xi(s_k)^*] \right\}. \end{aligned} \quad (\text{A7})$$

The scalar factor part can be rewritten in the form $\text{Im} [\xi(s') \xi(s)^*] = \frac{c^2}{\omega^3} \sin \omega(s' - s)$.

We now focus on the thermal average of the boson operator, $\exp \left\{ \sum_j \sigma_j r_j \xi(s_j) b^\dagger - \text{c.c.} \right\}$. The thermal average of free boson operator of the above form can be obtained as

$$\text{Tr}_b \left\{ \rho_b e^{\kappa b^\dagger - \kappa^* b} \right\} = \exp \left\{ -\frac{1}{2} \kappa \kappa^* \coth \left(\frac{\beta \omega}{2} \right) \right\}, \quad (\text{A8})$$

where $\rho_b = e^{-\beta H_b}$. We can take the thermal average of the two-time correlator to obtain

$$\begin{aligned} \text{Tr}_b \left\{ \rho_b \mathcal{B}_{\sigma'}^{r'}(s') \mathcal{B}_\sigma^r(s) \right\} = \\ \exp \left\{ \sigma' \sigma r' r \frac{c^2}{\omega^3} [1 - \cos \omega(s' - s)] \coth \left(\frac{\beta \omega}{2} \right) \right\} \times \\ \exp \left\{ i \sigma' \sigma r' r \frac{c^2}{\omega^3} \sin \omega(s' - s) \right\}, \end{aligned} \quad (\text{A9})$$

where a time-independent phase is dropped, since it cancels out when a configuration on the Keldysh contour is considered. By choosing $\sigma' = -1$ and $\sigma = 1$ and putting the ℓ index back, we can carry out \sum_ℓ in terms of spectral density $J(\omega)$,

$$\begin{aligned} \text{Tr}_b \left\{ \rho_b \mathcal{B}_-^{r'}(s') \mathcal{B}_+^r(s) \right\} = \\ \exp \left\{ r' r [-\mathcal{Q}_2(s' - s) - i \mathcal{Q}_1(s' - s)] \right\}, \end{aligned} \quad (\text{A10})$$

where \mathcal{Q}_1 and \mathcal{Q}_2 are defined by Eqs. (56) and (57). The two-time correlation function, Eq. (55), is then given by

$$C(s', s)^{r' r} \equiv \text{Tr}_b \left\{ \rho_b \mathcal{B}_-^{r'}(s') \mathcal{B}_+^r(s) \right\} \quad (\text{A11})$$

Finally, we take the thermal average of the multi-time correlator

$$\begin{aligned} \text{Tr}_b \left\{ \rho_b \prod_j \mathcal{B}_{\sigma_j}^{r_j}(s_j) \right\} = \exp \left\{ \sum_j \sum_{k < j} \sigma_j \sigma_k r_j r_k \frac{c^2}{\omega^3} [1 - \cos \omega(s_j - s_k)] \coth \left(\frac{\beta \omega}{2} \right) \right\} \times \\ \exp \left\{ i \sum_j \sum_{k < j} \sigma_j \sigma_k r_j r_k \frac{c^2}{\omega^3} \sin \omega(s_j - s_k) \right\}. \end{aligned} \quad (\text{A12})$$

We can finally carry out \sum_ℓ in terms of spectral density $J(\omega)$, concluding that

$$\text{Tr}_b \left\{ \rho_b \prod_j \mathcal{B}_{\sigma_j}^{r_j}(s_j) \right\} = \prod_j \prod_{k < j} (C(s_j, s_k)^{r_j r_k})^{-\sigma_j \sigma_k}. \quad (\text{A13})$$

Since we have $\sigma_j = 1$ for j even and $\sigma_j = -1$ for j odd, the powers are

$$-\sigma_j \sigma_k = \begin{cases} 1 & |j - k| \text{ odd} \\ -1 & |j - k| \text{ even} \end{cases}. \quad (\text{A14})$$

REFERENCES

- ¹A. Nitzan and M. A. Ratner, *Science* **300**, 1384 (2003).
- ²D. Fausti, R. Tobey, N. Dean, S. Kaiser, A. Dienst, M. C. Hoffmann, S. Pyon, T. Takayama, H. Takagi, and A. Cavalleri, *Science* **331**, 189 (2011).
- ³J. W. Negele and H. Orland, *Quantum many-particle systems*, Vol. 200 (Addison-Wesley New York, 1988).
- ⁴I. Bloch, J. Dalibard, and W. Zwerger, *Rev. Mod. Phys.* **80**, 885 (2008).
- ⁵S. Trotzky, L. Pollet, F. Gerbier, U. Schnorrberger, I. Bloch, N. V. Prokof'ev, B. Svistunov, and M. Troyer, *Nature Physics* **6**, 998 (2010).
- ⁶V. A. Kashurnikov, N. V. Prokof'ev, and B. V. Svistunov, *Phys. Rev. A* **66**, 031601 (2002).
- ⁷M. Troyer and U.-J. Wiese, *Phys. Rev. Lett.* **94**, 170201 (2005).
- ⁸E. Shakhnovich, G. Farztdinov, A. M. Gutin, and M. Karplus, *Phys. Rev. Lett.* **67**, 1665 (1991).
- ⁹M. J. Saxton, *Biophys. J.* **70**, 1250 (1996).
- ¹⁰N. Prokof'ev and B. Svistunov, *Phys. Rev. Lett.* **87**, 160601 (2001).
- ¹¹M. E. J. Newman and G. T. Barkema, *Monte Carlo Methods in Statistical Physics* (Oxford University Press: New York, USA, 1999).
- ¹²C. H. Mak and D. Chandler, *Phys. Rev. A* **41**, 5709 (1990).
- ¹³E. Burovski, N. Prokof'ev, B. Svistunov, and M. Troyer, *Phys. Rev. Lett.* **96**, 160402 (2006).
- ¹⁴J. E. Hirsch, R. L. Sugar, D. J. Scalapino, and R. Blankenbecler, *Phys. Rev. B* **26**, 5033 (1982).
- ¹⁵J. E. Hirsch, *Phys. Rev. B* **38**, 12023 (1988).
- ¹⁶R. Egger, L. Mühlbacher, and C. H. Mak, *Phys. Rev. E* **61**, 5961 (2000).
- ¹⁷T. Maier, M. Jarrell, T. Pruschke, and M. H. Hettler, *Reviews of Modern Physics* **77**, 1027 (2005).
- ¹⁸R. J. Needs, M. D. Towler, N. D. Drummond, and P. L. R. A. Os, *Journal of Physics: Condensed Matter* **22**, 023201 (2010).
- ¹⁹J. P. F. LeBlanc, A. E. Antipov, F. Becca, I. W. Bulik, G. K.-L. Chan, C.-M. Chung, Y. Deng, M. Ferrero, T. M. Henderson, C. A. Jiménez-Hoyos, E. Kozik, X.-W. Liu, A. J. Millis, N. V. Prokof'ev, M. Qin, G. E. Scuseria, H. Shi, B. V. Svistunov, L. F. Tocchio, I. S. Tupitsyn, S. R. White, S. Zhang, B.-X. Zheng, Z. Zhu, and E. Gull (Simons Collaboration on the Many-Electron Problem), *Phys. Rev. X* **5**, 041041 (2015).
- ²⁰S. Rombouts, K. Heyde, and N. Jachowicz, *Phys. Lett. A* **242**, 271 (1998).
- ²¹L. Mühlbacher and E. Rabani, *Phys. Rev. Lett.* **100**, 176403 (2008), 0707.0956.
- ²²M. Schiró, *Phys. Rev. B* **81**, 085126 (2010).

- ²³P. Werner, A. Comanac, L. De' Medici, M. Troyer, A. J. Millis, L. De Medici, M. Troyer, and A. J. Millis, Phys. Rev. Lett. **97**, 076405 (2006).
- ²⁴P. Werner and A. J. Millis, Phys. Rev. B **74**, 155107 (2006).
- ²⁵E. Gull, P. Werner, O. Parcollet, and M. Troyer, EPL (Europhysics Letters) **82**, 57003 (2008).
- ²⁶E. Gull, D. R. Reichman, and A. J. Millis, Phys. Rev. B **82**, 075109 (2010).
- ²⁷E. Gull, A. J. Millis, A. I. Lichtenstein, A. N. Rubtsov, M. Troyer, and P. Werner, Rev. Mod. Phys. **83**, 349 (2011), 1012.4474.
- ²⁸P. Werner, T. Oka, and A. J. Millis, Phys. Rev. B **79**, 035320 (2009).
- ²⁹P. Werner and A. J. Millis, Phys. Rev. Lett. **104**, 146401 (2010).
- ³⁰G. Cohen and E. Rabani, Phys. Rev. B **84**, 075150 (2011).
- ³¹G. Cohen, E. Y. Wilner, and E. Rabani, New Journal of Physics **15**, 073018 (2013).
- ³²G. Cohen, E. Gull, D. R. Reichman, A. J. Millis, and E. Rabani, Phys. Rev. B **87**, 195108 (2013).
- ³³R. Egger and U. Weiss, Zeitschrift für Phys. B Condens. Matter **89**, 97 (1992).
- ³⁴R. Egger and C. H. Mak, Phys. Rev. B **50**, 210 (1994).
- ³⁵L. Mühlbacher and R. Egger, J. Chem. Phys. **118**, 179 (2003).
- ³⁶G. Cohen, E. Gull, D. R. Reichman, and A. J. Millis, Phys. Rev. Lett. **112**, 146802 (2014).
- ³⁷G. Cohen, D. R. Reichman, A. J. Millis, and E. Gull, Phys. Rev. B **89**, 115139 (2014).
- ³⁸G. Cohen, E. Gull, D. R. Reichman, and A. J. Millis, Phys. Rev. Lett. **115**, 266802 (2015).
- ³⁹A. J. Leggett, S. Chakravarty, A. T. A. Dorsey, M. P. A. Fisher, A. Garg, and W. Zwerger, Rev. Mod. Phys. **59**, 1 (1987).
- ⁴⁰U. Weiss, *Quantum dissipative systems*, Vol. 10 (World Scientific Publishing Company Incorporated, 1999).
- ⁴¹A. Nitzan, *Chemical Dynamics in Condensed Phases: Relaxation, Transfer, and Reactions in Condensed Molecular Systems* (Oxford University Press, New York, 2006).
- ⁴²H. Wang, M. Thoss, and W. H. Miller, J. Chem. Phys. **115**, 2979 (2001).
- ⁴³M. Thoss, H. Wang, and W. H. Miller, J. Chem. Phys. **115**, 2991 (2001).
- ⁴⁴H. Wang and M. Thoss, J. Chem. Phys. **119**, 1289 (2003).
- ⁴⁵C. H. Mak and R. Egger, *Adv. Chem. Physics, New Methods Comput. Quantum Mech.*, Vol. XCIII (John Wiley & Sons, Inc., 2007) pp. 39–76.
- ⁴⁶D. E. Makarov and N. Makri, Chem. Phys. Lett. **221**, 482 (1994).
- ⁴⁷N. Makri, J. Math. Phys. **36**, 2430 (1995).
- ⁴⁸Y. Tanimura and R. Kubo, J. Phys. Soc. Japan (1989).
- ⁴⁹J. Strümpfer and K. Schulten, J. Chem. Theory Comput. **8**, 2808 (2012).
- ⁵⁰N. Van Kampen, Physica **74**, 215 (1974).
- ⁵¹B. Yoon, J. Deutch, and J. H. Freed, J. Chem. Phys. **62**, 4687 (1975).
- ⁵²S. Mukamel, Chem. Phys. **37**, 33 (1979).
- ⁵³D. R. Reichman, F. L. H. Brown, and P. Neu, Phys. Rev. E **55**, 2328 (1997).
- ⁵⁴N. Metropolis, A. W. Rosenbluth, M. N. Rosenbluth, A. H. Teller, and E. Teller, J. Chem. Phys. **21**, 1087 (1953).
- ⁵⁵W. K. Hastings, Biometrika **57**, 97 (1970).
- ⁵⁶A. E. Antipov, Q. Dong, and E. Gull, Phys. Rev. Lett. **116**, 036801 (2016).
- ⁵⁷P. Werner and A. J. Millis, Phys. Rev. Lett. **99**, 146404 (2007).
- ⁵⁸P. Werner and M. Eckstein, Phys. Rev. B **88**, 165108 (2013).
- ⁵⁹H.-T. Chen, G. Cohen, A. J. Millis, and D. R. Reichman, Physical Review B **93**, 174309 (2016).
- ⁶⁰R. E. Profumo, C. Groth, L. Messio, O. Parcollet, and X. Waintal, Phys. Rev. B **91**, 245154 (2015).